OER Catalyst Stability Investigation Using RDE Technique: A Stability Measure or an Artifact?

OER Catalyst Stability Investigation Using RDE Technique: A Stability Measure or an Artifact?

Hany A. El-Sayed,[z] Alexandra Weiß,[*] Lorenz F. Olbrich, Garin P. Putro, and Hubert A. Gasteiger[**]

Chair of Technical Electrochemistry, Technical University of Munich, D-85748, Garching, Germany

The rotating disk electrode (RDE) technique was frequently used for investigating the stability of oxygen evolution reaction (OER) catalysts under galvanostatic conditions, where the increase in potential is reported to be due to catalyst degradation. The galvanostatic RDE stability test typically results in catalyst life-time of several hours, although the same catalyst can last for thousands of hours in a PEM electrolyzer under similar conditions, a discrepancy that is still unresolved. In this work, we present a careful examination of the use of the RDE technique as a tool for the investigation of the OER catalyst stability. Our findings provide a clear evidence that the change in potential during the stability test is not related at all to catalyst degradation, but is rather due to an experimental artifact caused by nano- and micro-bubbles formed within the pores of the catalyst layer during the OER, which cannot be removed by electrode rotation. Instead, they accumulate and shield the OER active sites from the electrolyte, resulting in an increase of the potential, which is mistakenly interpreted as catalyst degradation in previous literature. Thus, reliable OER catalyst stability tests other than testing in a real electrolyzer cell still needs to be designed.

 [DOI: 10.1149/2.0301908jes]

Manuscript submitted February 14, 2019; revised manuscript received April 1, 2019. Published April 23, 2019.

The development of oxygen evolution reaction (OER) catalysts for polymer electrolyte membrane water electrolysis (PEMWE) requires the use of reliable methods for both activity and stability testing. To date, IrO_x-based materials, state-of-the-art catalysts for OER in acidic media, have been optimized for the highest OER activity through controlling catalyst morphology and the type of the oxide support.[1–5]

It is very well-established that the OER catalyst activity can be reliably estimated by using rotating disk electrode (RDE) or flow-channel methods in half-cells or by full-cell testing in an electrolyzer.[6–12] On the other hand, the evaluation of OER catalyst stability over the whole lifetime under realistic conditions is not practical, as the current industrial life-time targets are five to ten years.[13] Therefore, accelerated degradation tests using cells with liquid electrolyte or actual proton exchange membrane (PEM) electrolyzer are performed in order to carry out comparative stability studies of various catalysts.[14–19] A protocol for the OER catalyst stability using RDE was proposed by the Joint Center for Artificial Photosynthesis (JCAP) group and is now frequently used by other research groups.[20] In this protocol, OER catalyst stability is determined using galvanostatic electrolysis, where a constant current (e.g., 10 mA/cm^2_{disk}) is applied in a RDE configuration at a constant rotation rate of 1600 RPM and the change in potential as a function of time is monitored for a few hours.[20] The increase of the potential during the test is considered as an evidence of catalyst "deactivation", while a steady potential indicates a stable catalyst. The authors indicated that this stability protocol does not distinguish between the various mechanisms of catalyst deactivation; like corrosion, material degradation, or surface passivation.

This protocol was then used by other researchers to compare the stability of their developed OER catalysts against reference materials. For example, Oh et al. reported the enhanced stability of antimony-doped tin oxide (ATO)-supported Ir nanodendrites (ND) over all of their investigated reference catalysts, including carbon-supported Ir nanoparticles, Ir-black, Ir-ND, and Ir-ND/C.[21] The authors reported that when a constant current density of 10 mA/cm^2_{disk} is applied on all of the catalysts, all reference materials showed a gradual increase of the potential as a function of time, followed by a sudden potential jump, which the authors considered an indication of complete catalyst degradation.[21] Only Ir-ND/ATO showed a very small increase in potential for 15 hours without any potential jump, suggesting the superior stability of this catalyst compared to the reference materials.[21] Using the same protocol, Oh et al. reported another study on the existence of the strong metal-support interaction (SMSI) in IrO_x/ATO (compared to IrO_x/C).[18] In that study, the absence of a potential jump over 15 hours of testing in case of IrO_x/ATO and the observation of a potential jump after 10 hours for IrO_x/C was interpreted by the authors to indicate a superior stability of IrO_x/ATO vs. IrO_x/C, which may attribute to the SMSI effects. Wang et al. also used the same approach and concluded on the superior stability of their developed aerogel catalyst (Ir/SnO_2:Sb-mod-V) over conventional catalysts, again using the potential jump as an indication of full catalyst degradation.[22] Zhang et al. reported the stability test of Ir catalyst anchored on 3D graphite foam using the same RDE stability protocol, where no potential jump was observed up to 10 hours for the developed catalyst, with no comparison to any reference material.[23]

Geiger et al. noticed that the galvanostatic RDE stability test overlooks many aspects and that the catalyst life-time defined by the potential jump is inconsistent with stability results from a PEM electrolyzer, in which a catalyst can be stable under similar operating conditions (current density, pH, temperature, etc.) for ten thousands of hours. The discrepancy indicates that this RDE stability test may have some limitations.[13] Furthermore, they showed that the catalyst life-time, measured by RDE, depends on the nature of the electrode substrate on which the catalyst powder is being supported. Specifically, it was suggested that the potential jump, used as an indicator of full catalyst degradation, is actually due to glassy carbon passivation, making the catalyst no longer electrochemically accessible due to the high contact resistance, ultimately leading to the sudden potential jump. Consequently, other electrode substrates were tested to avoid materials that passivate at high potential, and it was recommended that gold and boron-doped diamond should be used as they show better stability of the catalyst under investigation, while glassy carbon and fluorine-doped tin oxide electrodes were deemed unsuitable for such stability tests.[13] Although Geiger et al. found that the potential jump depends on the electrode substrate, the results still do not explain the inconsistency between stability results from an electrolyzer and those from an RDE test.

In general, the potential increase during a galvanostatic RDE stability test can result from passivation of the RDE electrode substrate, from catalyst degradation (dissolution), from physical detachment of catalyst material or from the accumulation of oxygen bubbles. In this study, a homemade iridium catalyst supported on antimony-doped tin oxide (ATO), recently reported to provide extremely high OER activity,[8] is used to identify the main cause for the potential increase in a galvanostatic stability test and to conclude whether the galvanostatic RDE

*Electrochemical Society Student Member.
**Electrochemical Society Fellow.
[z]E-mail: hany.el-sayed@tum.de

stability test is a reliable technique to determine the stability of OER catalysts.

Experimental

ATO support synthesis.—Following the procedure developed by Beyer et al., antimony-doped tin oxide (ATO) with a molar Sb:Sn ratio of 5:95 is prepared in an open 100 ml autoclave with a PTFE liner (HighPreactor BR-100, Berghof), where 30.0 ml concentrated HNO_3 (69 wt%, puriss. p.a., Sigma Aldrich) are added to 50.0 ml deionized water. 2.0 g tin (16.9 mmol, Sn, granulates, 0.425-2.0 mm, $\geq$ 99.5%, ACS reagent, Sigma Aldrich) and 130 mg antimony(III) oxide powder (0.440 mmol, Sb_2O_3, nanopowder, $<$ 250 nm, $\geq$ 99.9%, Sigma Aldrich) are added at once to the acidic solution under vigorous stirring.[30] After 10 minutes, the autoclave is sealed and heated to 140°C at a heating rate of 2°C/min. This temperature is held for 10 h, followed by cooling the reaction mixture passively to room temperature. A bluish powder is obtained and separated from the liquid phase by centrifugation. The powder is washed thoroughly with deionized water until the washing water reaches pH 6. After the final washing step with ethanol, the powder is dried overnight in static air at 70°C. The resulting dry powder is calcined in a tube furnace (Carbolite) in a gas flow of 20% O_2 in Ar (both 5.0-grade, Westfalen) with a flow rate of 400 ml/min. The samples are heated to 600°C at 5°C/min and held at 600°C for 3 h. After passive cool down to room temperature in the furnace, the calcined samples are ground in a planetary ball mill (Pulverisette 7 Premium Line, Fritsch) in order to break up the formed agglomerates during calcination. In this process, ca. 2 g of ATO are suspended in 6 ml isopropanol and filled into a 45 ml ZrO_2 milling jar containing 20 ZrO_2 balls (Ø 10 mm). Six milling cycles of 10 min each and 1 min pause between the cycles are conducted at 200 rpm. Again, the product is separated by centrifugation and dried overnight at 70°C in static air.

Synthesis of Ir nanoparticles.—The polyol synthesis setup consists of a 100 ml three-neck flask with magnetic stirrer placed in a heating mantel (WHG 2, Winkler), equipped with a reflux condenser, a thermometer, and a temperature controller (Model 310, J-KEM Scientific). Additionally, there is a glass capillary, which is connected to a high purity argon supply (5.0-grade, Westfalen). The whole system is sealed off with septa. In a typical polyol synthesis, 183 mg dihydrogen hexachloroiridate(IV) hydrate (0.450 mmol, H_2IrCl_6 x H_2O, 99.98%, trace metal basis, Sigma Aldrich) are dissolved in 10 ml ethylene glycol (EG, 99.8%, anhydrous, Sigma Aldrich) in a small vial at room temperature under vigorous stirring. After complete dissolution, the solution is transferred into a three-neck flask with another 80 ml of ethylene glycol. The total iridium concentration is $5 \cdot 10^{-3}$ mol/l in a total volume of 90 ml. The solution is purged with argon for 60 min in order to minimize the O_2 content before heating. During heating, the solution is stirred moderately (at approx. 500 RPM) under argon. The solution is heated up to 140°C at a heating rate of approx. 2°C/min, where it is held for one hour, after which time the reaction mixture is allowed to cool down to room temperature.

Preparation of ATO-supported iridium catalysts.—The prepared iridium nanoparticles are slowly added to the ATO suspended in 35 ml ethylene glycol by sonication for at least 30 min. The reaction mixture is stirred at 500 RPM at room temperature under air for three days until all the nanoparticles are deposited on the ATO. Afterwards, the prepared catalyst is separated via centrifugation at 11500 RPM and 5°C, and washed twice with isopropanol with 5 min sonication in between the centrifugation steps. The obtained black powder is dried at 70°C in static air overnight. The morphology and composition of the final catalyst was confirmed using transmission electron microscopy (Philips CM100 EM) and energy dispersive X-ray analysis (JCM-6000Plus from JEOL).

Electrochemical setup and measurement procedure.—The electrochemical measurements (cyclic voltammetry, galvanostatic polarization, and electrochemical impedance spectroscopy (EIS)) were performed in a glass three-electrode electrochemical cell. A reversible hydrogen electrode (RHE) and a high surface area Au wire were used as reference and counter electrodes, respectively. The RHE reference electrode was either directly connected to the cell or via a Luggin capillary. Rotating ring-disk electrodes (RRDEs) with a 5 mm diameter polycrystalline gold (Au) electrode and a Pt ring supported by a PTFE-body (Pine Research Instrumentation, USA) were used as working electrodes. The reference potential was calibrated in H_2-saturated electrolyte prior to every experiment using the platinum ring of the RRDE and all potentials in this publication are given with respect to RHE.

Electrolyte solutions were prepared from high purity H_2SO_4 (Ultrapur, 96%, Merck Millipore KGaA, Germany) by addition of ultrapure water (18.2 MΩ.cm at 20°C, Merck Millipore KGaA, Germany). Ar, O_2, and H_2 used for purging of the electrolyte were of high purity (6.0-grade, Westfalen AG).

Electrochemical measurements were performed using an Autolab potentiostat (PGSTAT302N, Metrohm AG) and a rotator (Pine Research Instrumentation) with a polyether ether ketone shaft. Prior to any electrochemical measurements, a cyclic voltammogram of the gold working electrode was recorded in the supporting electrolyte to verify the cleanliness of the Au disk and the cell. Afterwards, the electrode was removed, dried, and coated with the catalyst ink that was allowed to dry under a low flow of nitrogen.

The coated electrode was then dipped into the Ar-purged electrolyte and the electrolyte resistance between reference and working electrode was determined by EIS from 100 kHz to 100 Hz at open circuit potential (OCP) with an amplitude of 10 mV. The potential was then cycled at least 20 times between 0.05 and 1.45 V RHE at 100 mV/s to convert all metallic iridium into (hydrous) iridium oxide. Afterwards, the electrolyte solution was replaced by fresh 0.1 M H_2SO_4 and saturated with O_2. After fully saturating the electrolyte with O_2, polarization curves were recorded from 1.2 V_{RHE} to 1.7 V_{RHE} at 10 mV/s at a rotation rate of 2500 RPM. Galvanostatic experiments were carried out directly after the linear polarization curves, whereby a constant current density was applied and the resulting potential was recorded over time.

Electrode and ink preparation.—Prior to every measurement, the Au working electrode was polished with 0.3 μm Al_2O_3 polishing suspension (Buhler AG) and sonicated various times in ultrapure water. Inks were prepared by adding ultrapure water to the dry catalyst (11 wt% Ir/ATO) to obtain a catalyst ink concentration of 1 mg_{Cat}/1 ml. The catalyst suspension was sonicated for 30 min in a sonication bath (Elmasonic S 30 H, Elma Schmidbauer GmbH) to achieve a homogeneous dispersion. The temperature of the bath was maintained at less than 35°C to avoid evaporation of the solvent. No polymeric binder was added to the catalyst suspension.

Results and Discussion

Fig. 1a shows a typical OER polarization curve (iR-corrected) of 11 wt% Ir/ATO catalyst (deposited on a gold disk) in O_2-saturated 0.1M H_2SO_4 solution at 20 mV/s and 2500 RPM, while Fig. 1b shows a galvanostatic stability test obtained by applying a mass-specific current density of 1 mA/μg_{Ir} for a catalyst loading of 5.50 $\mu g_{Ir}/cm^2_{disk}$ (equivalent to 5.50 mA/cm^2_{disk}) for several hours. It can be seen that the starting potential (1.57 V) of the potential-time transient at 5.50 $\mu g_{Ir}/cm^2_{disk}$ (see Fig. 1b) fits reasonably well with the potential obtained at the same current density (1.55 V) for a conventional RDE experiment (see orange line in Fig. 1a). The potential gradually increases with time, which according to the literature indicates a degradation of the catalyst layer until its complete degradation once the potential jump is observed. At that point, a constant potential of ca. 2.12 V is observed, most likely due to the OER taking place solely on the Au substrate after catalyst degradation. The catalyst was found to be stable for 20 hours under these conditions, but when the applied current density was increased from 5.50 to 16.5 mA/cm^2_{disk}

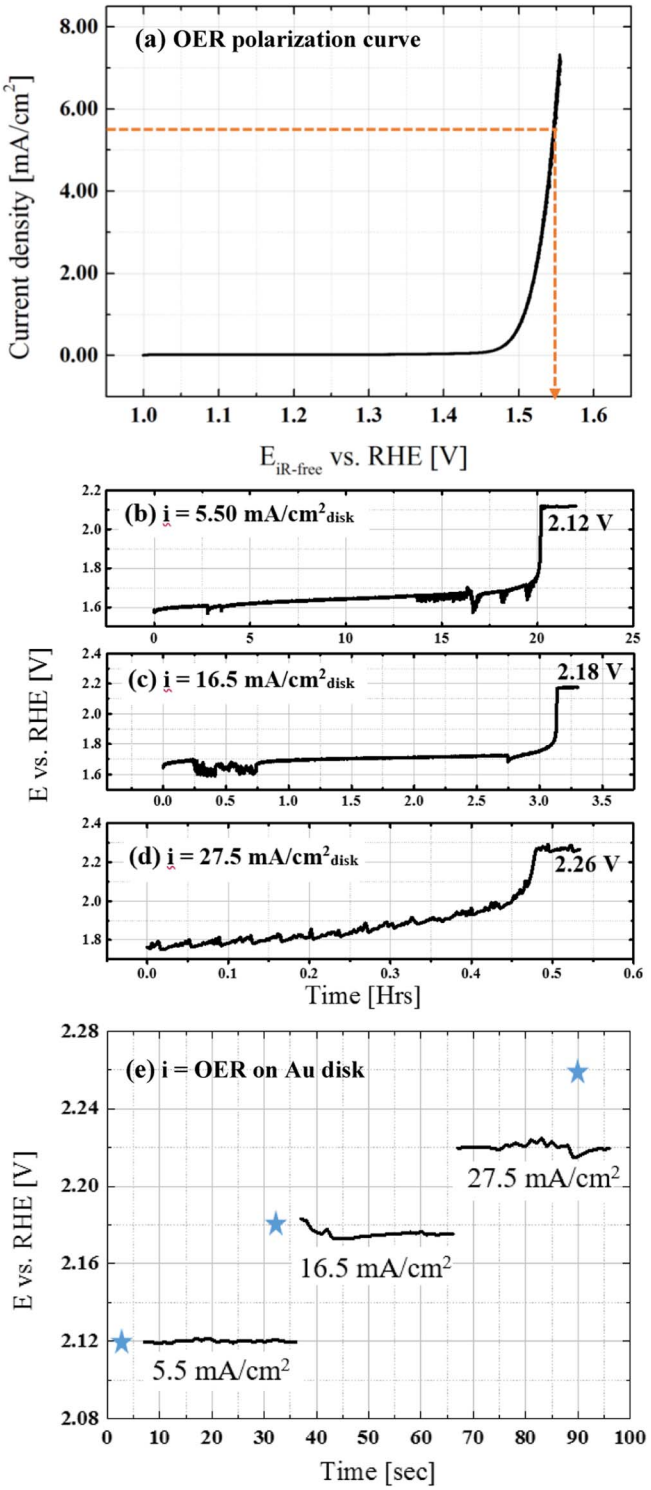

Figure 1. OER polarization curve (20 mV/s) (a) and galvanostatic stability transients at (b) 5.50 mA/cm$^2_{disk}$, (c) 16.5 mA/cm$^2_{disk}$, and (d) 27.5 mA/cm$^2_{disk}$ for an 11 wt% Ir/ATO catalyst in O_2-saturated 0.1 M H_2SO_4 at 2500 RPM and 25°C. Catalyst loading is 5.50 μg_{Ir}/cm$^2_{disk}$ on a polycrystalline Au electrode. (e) Potential at different current densities obtained under the same conditions for a polycrystalline Au disk without catalyst, with the blue asterisks indicating the potential obtained after the potential jump in (b-d).

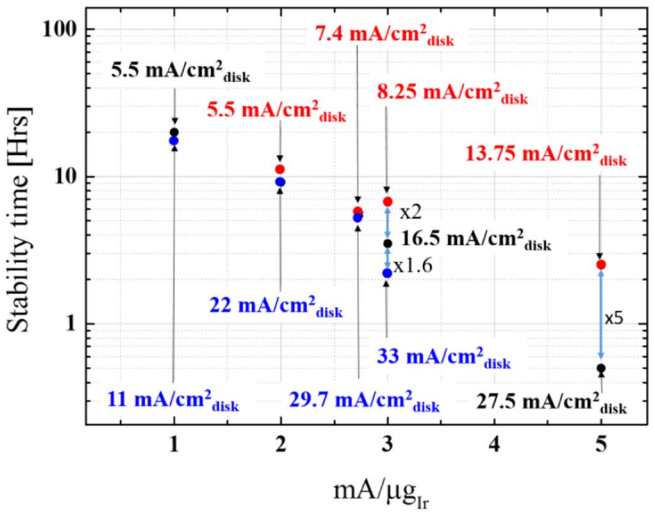

Figure 2. Effect of catalyst loading (2.75 μg_{Ir}/cm$^2_{disk}$ (red dots), 5.50 μg_{Ir}/cm$^2_{disk}$ (black dots), and 11.0 μg_{Ir}/cm$^2_{disk}$ (blue dots)), and mass-specific current density on catalyst stability.

(i.e., from 1 to 3 mA/μg_{Ir}), the catalyst was stable for only 3.5 hours as shown in Fig. 1c. Increasing the applied current even further to 27.5 mA/cm$^2_{disk}$ (i.e., to 5 mA/μg_{Ir}), the catalyst was stable for only 30 min (see Fig. 1d). In all cases, the overall behavior is the same: first, a gradual increase in potential, followed by a potential jump and a final potential plateau. To confirm that the final potential plateaus are indeed due to the OER on the Au substrate, the same current densities (5.50, 16.5, and 27.5 mA/cm$^2_{disk}$) were applied to the Au electrode in the absence of any catalyst, and the corresponding potentials (black lines in Fig. 1e) were compared to the final potential plateaus (indicated by blue stars in Figs. 1e). The reasonably close agreement between these potential values confirms that after the potential jump there either is no catalyst remaining on the electrode substrate or that the catalyst becomes electrically completely disconnected from the Au surface and therefore electrochemically inaccessible.

These results so far suggest that when the catalyst loading on the disk is kept constant (5.50 μg_{Ir}/cm$^2_{disk}$ in this case), the larger the applied current, the higher is the catalyst degradation rate, which supports the results reported in the literature where the OER stability test is mostly considered a suitable tool to quantify OER catalyst stability. If this were to be correct and if the potential increase is indeed due to catalyst degradation, then the degradation rate for a specific catalyst should be dependent only on the applied mass-specific current density (current per OER active site) and not on the geometric current density. This, however, cannot be confirmed by the results shown in Figs. 1a–1d, as both mass-specific current density and geometric current density vary simultaneously.

To deconvolute the effects of geometric (mA/cm$^2_{disk}$) and mass-specific (mA/μg_{Ir}) current densities, the catalyst loading on the disk was changed (2.75, 5.50, and 11.0 μg_{Ir}/cm$^2_{disk}$) while fixing the mass-specific current density by varying the geometric current density. This should result in the same stability time, if the degradation rate is dependent only on the mass-specific current density. Surprisingly, Fig. 2 shows that when the catalyst loading on the disk was changed from 5.50 μg_{Ir}/cm$^2_{disk}$ (black dots) to 2.75 μg_{Ir}/cm$^2_{disk}$ (red dots), a 5-fold increase in the stability was obtained when a constant current of 5 mA/μg_{Ir} was applied. Decreasing the catalyst loading while maintaining the applied mass-specific current density results in a lower geometric current density, therefore decreasing the overall rate of O_2 production. This may indicate that the created oxygen bubbles are somehow influencing the stability time by shielding the OER active sites from the electrolyte, where a lower O_2 evolution rate seems to result in a longer stability time (see Fig. 2). The same behavior was observed for 3 mA/μg_{Ir}, where the catalyst loading on the disk

was decreased from 5.50 $\mu g_{Ir}/cm^2_{disk}$ (black dots) to 2.75 $\mu g_{Ir}/cm^2_{disk}$ (red dots), leading to a two-fold increase in the stability time for the lower catalyst loading. Increasing the catalyst loading on the disk from 5.50 $\mu g_{Ir}/cm^2_{disk}$ (black dots) to 11.0 $\mu g_{Ir}/cm^2_{disk}$ (blue dots), while applying the same mass-specific current density of 3 mA/μg_{Ir} resulted in a 1.6-fold decrease of the stability time, again showing higher stability for a lower catalyst loading. The influence of the catalyst loading at constant mass-specific current density on the stability time decreased from 5 mA/μg_{Ir} to 3 mA/μg_{Ir}, which is most likely due to the decrease in the O_2 evolution rate. When the O_2 evolution rate (i.e., the geometric current density) was further decreased by applying 2.75 mA/μg_{Ir} using loadings of either 2.75 $\mu g_{Ir}/cm^2_{disk}$ (red dots) or 11.0 $\mu g_{Ir}/cm^2_{disk}$ (blue dots), no significant change in stability time was observed. This was also observed for mass-specific current densities of 1 mA/μg_{Ir} and 2 mA/μg_{Ir}, suggesting that the influence of the evolved O_2 bubbles on the stability time is much smaller at low mass-specific current densities, which generally means at low catalyst loadings or of low geometric current densities. If the O_2 bubbles formed during the galvanostatic RDE-based OER stability test are at least partially responsible for the potential increase, they should have a similar effect on the linear scan polarization curves of the catalyst during OER activity determination, i.e., the activity should decrease as a function of the cycle number due to the gradual accumulation of oxygen bubbles.

Figure 3a shows mass-specific OER polarization curves (iR-corrected) of 11 wt% Ir/ATO catalyst (deposited on a Au electrode) in O_2-saturated 0.1 M H_2SO_4 at 10 mV/s, 25^{0}C, and 2500 RPM, where it can be seen that the OER currents decrease upon potential cycling (1.4 – 1.55 V_{RHE}). This decrease cannot be attributed to the passivation of the Au disk substarte, as Au passivation at the upper scan potential of 1.7 V is limited to a monolayer of Au oxide,[24] which does not impose a significant resistance. The physical detachment of the catalyst material is also excluded, as it usually would result in a sudden and arbitrary decrease in the current upon cycling, which was not observed here. Thus, the gradual decrease of the OER current upon potential cycling is either due to catalyst degradation or due to the gradual accumulation of oxygen gas bubbles within the pores of the catalyst layer, thereby blocking electrolyte access to a fraction of the OER active sites.

To distinguish between these two possibilities, the RDE setup was purged with Ar for 30 min directly after the OER testing (Fig. 3a) while switching the electrode to OCP (open circuit potential), then this was followed by taking another polarization curve under O_2 atmosphere. This experiment is designed based on the assumption that during the OER, oxygen bubbles are formed on the catalyst layer surface as well as within the pores of the layer. While the nano- and micro-bubbles that form inside the catalyst layer can obviously not be removed by convection (i.e., rotation), contrary to the macro-bubbles that are formed on top of the catalyst layer and can be removed by convection, they could be removed by oxygen diffusion into the bulk of the electrolyte. However, even if the OER experiment were carried out under Ar atmosphere, the electrolyte in the vicinity of the catalyst layer would be saturated with O_2 produced by the OER, so that removal of O_2 bubbles via dissolution and diffusion cannot occur. On the other hand, once the electrode is put into OCP and once the RDE setup is purged with Ar, O_2 bubbles can be removed via dissolution and diffusion. This effect is explored in the experiments shown in Fig. 3. In Fig. 3a, the potential control was stopped and the electrode was kept under OCP, while the solution was purged with Ar at 2500 RPM. If the accumulation of bubbles were the main cause for the "apparent degradation", some or all (depending on time) of the oxygen should be removed from the catalyst layer by diffusion. Fig. 3b shows three polarization curves, initial (2nd cycle), after 30 cycles, and after Ar purging, all recorded under O_2 atmosphere. It can be clearly seen that Ar purging recovers part of the activity lost after 30 cycles. For example, at 1.5 V_{RHE}, the initial OER activity was found to be 172 A/g_{Ir} (black line in Fig. 3b), and decreased to 88 A/g_{Ir} after 30 cycles (blue line in Fig. 3b), i.e., ca 50% of the OER activity was lost. After Ar purging for 30 min, the OER activity recovered to 122 A/g_{Ir} (red line in Fig. 3b), i.e., 40% of the lost activity was regained. These results suggest that the nano- and

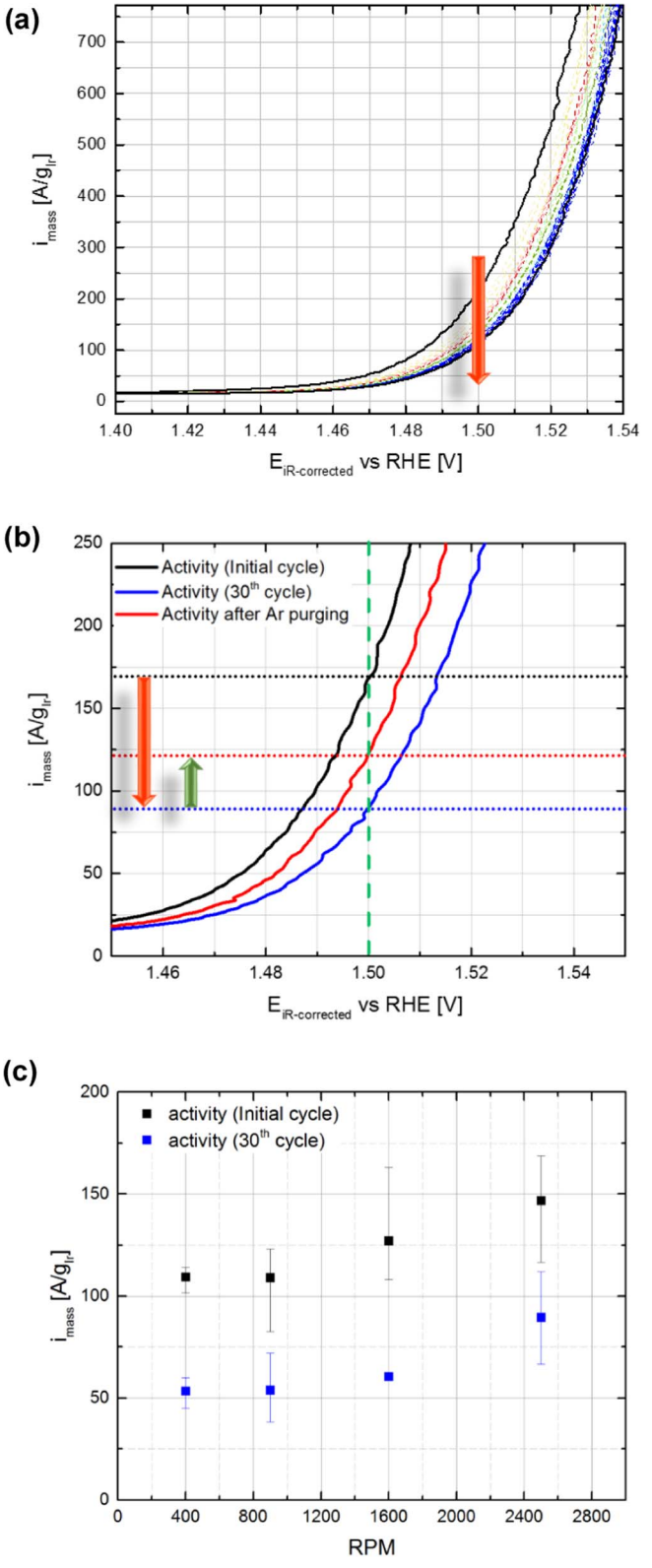

Figure 3. Mass-specific OER polarization curves (iR-corrected) of the 11 wt% Ir/ATO catalyst (deposited on a Au electrode) in O_2-saturated 0.1 M H_2SO_4 at 10 mV/s, 25^{0}C, and 2500 RPM. The catalyst loading was 22.4 $\mu g_{Ir}/cm^2_{disk}$, and the potential was cycled between 1.2 and 1.7 V vs. RHE (a) for 30 cycles, and (b) before (initial and 30th cycle) and after Ar purging for 30 min at OCP. (c) Effect of RPM on the OER mass-specific activities measured at 1.5 V_{RHE} from initial and 30th cycles.

micro-bubbles within the pores of the catalyst layer are responsible for the current decrease during potential cycling.

To examine the hypothesis of the blockage by O_2 bubbles, the OER polarization curves were measured at 400–2500 RPM and the current decay (at 1.5 V_{RHE}) as a function of potential cycle number was observed. Each rotation speed was studied using a freshly catalyst-coated Au electrode, where a catalyst loaing of 22.4 $\mu g_{Ir}/cm^2_{disk}$ was used. Fig. 3c shows that the OER activity determined at 1.5 V_{RHE} from the initial cycle depends on the rotation rate where it decreases by decreasing the rotation rate. This clearly indicates that the accumulation of bubbles within the porosity of the catalyst layer occurs from the very beginning of the experiment and that its effect on OER activity can be even observed at the initial cycle. The same behavior was also observed for OER activities determined from the 30th cycle, where the highest OER activity was reported at 2500 RPM (ca. 83 A/g_{Ir}), which is about 50% of that reported at the same RPM from the initial cycle (ca. 150 A/g_{Ir}).

To verify whether the accumulation of O_2 bubbles within the pores of the catalyst layer is responsible for the typical potential increase during a galvanostatic stability test, the Ir/ATO catalyst was subjected to a constant OER current and the experiment was stopped once a pre-defined potential increase was reached. This experiment is based on the assumption that if the potential increase over galvanostatic aging were mainly due to catalyst degradation, as suggested by many researchers in the literature, the correlation between the measured potential increase and the available OER active sites would have to be consistent with the Tafel equation. And hence, the available active surface area of the catalyst over the course of the experiment, i.e., the roughness factor (*rf*) of the catalyst layer supported on the RDE substrate (in units of $cm^2_{cat.}/cm^2_{disk}$), would have to be directly correlated to the kinetic OER overpotential (η, given in mV):

$$\eta = TS \cdot \log\left(\frac{i}{i_0}\right) - TS.\log(rf) \qquad [1]$$

where, *TS* is the Tafel slope in mV/dec, *i* is the geometric OER current density in mA/cm^2_{disk}, and i_0 is the exchange current density of the catalyst for the OER in $mA/cm^2_{Cat.}$. Since in the galvanostatic aging test the current density *i* is constant, as is the catalyst exchange current density i_0, η would only depend on the effective roughness factor *rf* as described by the second term on the right-hand-side of equation 1. The roughness factor, in turn, could decrease by catalyst dissolution or by the ionic disconnection of the catalyst by trapped O_2 bubbles.

For example, for a potential increase that is equivalent to one Tafel slope (TS), there should be a corresponding 10-fold decrease in the number of OER active sites (i.e., a 10-fold decrease of the *rf*). As the TS of Ir/ATO catalysts has been reported to be around 45 mV/dec,[8] the galvanostatic stability test was designed in a way to allow the potential to increase by one TS (45 mV) from the starting potential. The system was then purged with Ar under OCP for 30 min to allow O_2 bubbles to diffuse away from the pores of the catalyst layer, while maintaining the 2500 RPM rotation, and then a CV was measured under Ar and compared to the pristine CV. This approach was applied after different potential increases of 1x TS (45 mV), 2x TS (90 mV), 3x TS (135 mV), and after the potential jump was observed. Each potential increase experiment was conducted using a freshly prepared electrode with an identical loading of 11.2 $\mu g_{Ir}/cm^2_{disk}$. In all cases, the CV obtained under Ar after the stability test was compared to that before the stability test. Fig. 4a shows that, when a constant current density of 11.2 mA/cm^2_{disk} is applied (corresponding to 1 $mA/\mu g_{Ir}$), an initial potential of 1.6 V_{RHE} was reproducibly obtained for all measurements and that the same gradual increase in potential with time was observed for all samples. Fig. 4b shows all CVs collected after a 30 min of Ar purging at OCP carried out directly after a given potential increase was reached; a CV of the pristine catalyst is given for reference. If the gradual change in potential were mainly due to catalyst degradation, an increase in potential of one TS should result in a 10-fold loss of catalyst surface area, i.e., in a 10-times smaller CV compared to the pristine CV. Analogously, for potential increases corresponding to 2x TS or 3x TS, only 1% or 0.1% of the catalyst surface area should be remaining after the stability test, and therefore their corresponding CVs should be 100- or 1000-times smaller than the pristine CV. After the potential jump, no active catalyst surface area should be left, and only the characteristic CV of the gold substrate should be obtained. However, Fig. 4b clearly shows that all CVs exhibit the main set of redox peaks centered at around 0.95 V, which is due to the Ir^{3+}/Ir^{4+} redox reaction. Surprisingly, none of the CVs shows the surface area loss which would be expected if the potential gain during the galvanostatic aging test were due to catalyst degradation/dissolution. Specifically, the CV obtained after a potential increase of one TS (blue line in Fig. 4b) would be expected to be an order of magnitude smaller than that of the pristine CV (black line in Fig. 4b). In fact, the results clearly show that there is almost no loss of catalyst surface area observed in this case, as the CVs are almost identical. By the same argument, the CVs obtained after potential increases corresponding to 2 TS and 3TS values could be expected to be two and three orders of

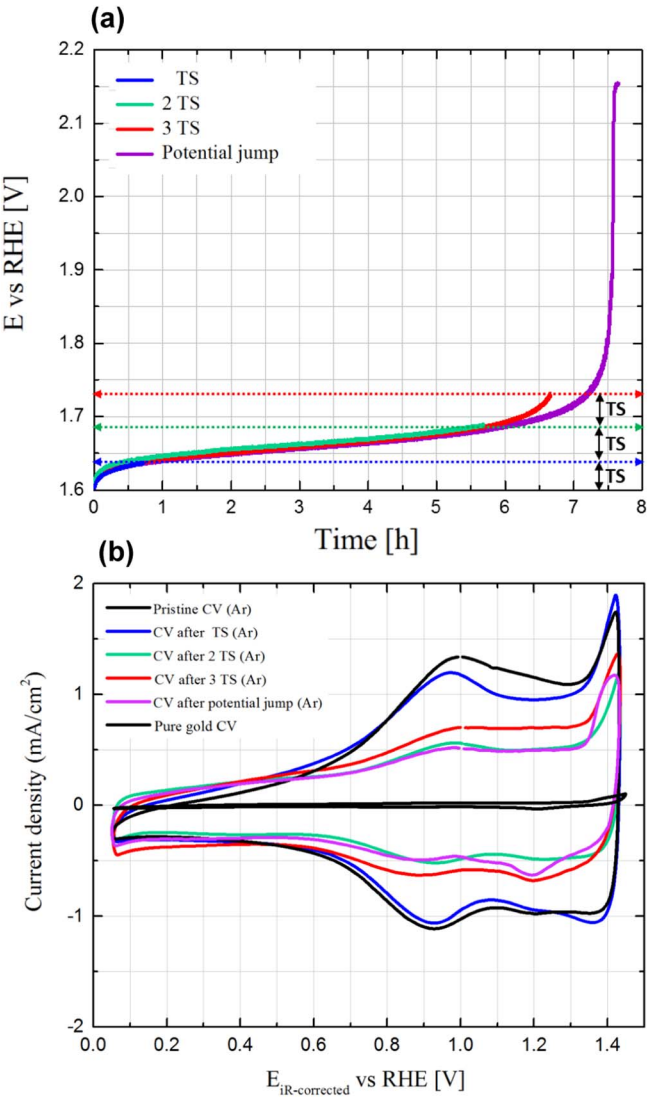

Figure 4. (a) Potential evolution vs. time in galvanostatic stability tests at 11.2 mA/cm^2_{disk} and 2500 RPM for 11 wt% Ir/ATO catalyst in O_2-saturated 0.1 M H_2SO_4 with catalyst loading of 11.2 $\mu g_{Ir}/cm^2_{disk}$ (≡ 1 $mA/\mu g_{Ir}$) until the potential has increased to 45 mV (≡ TS; blue line), 90 mV (≡ 2 TS; green line), 135 mV (≡ 3TS; red line), and to its final value after the potential jump (by roughly 550 mV). A fresh catalyst smple was used for each experiment. (b) Corresponding CVs after the stability tests and after 30 min hold at OCP under Ar at 2500 RPM, taken in Ar-saturated 0.1 M H_2SO_4 at 100 mV/s at 0 RPM.

magnitude smaller than that of the pristine CV, respectively. However, they are only ca. 50% smaller than the initial CV. In addition, even the CV obtained after the potential jump shows that ca. 50% of the catalyst surface area of the pristine catalyst is still remaining. These results clearly show that the potential increase during the galvanostatic stability test has nothing to do with catalyst surface area loss due to degradation/dissolution, and that the apparent OER activity loss is mainly due to an artifact of O_2 bubbles accumulating in the pores of the catalyst layer. The displacement of electrolyte within/near the catalyst layer by evolved oxygen apparently leads to a loss of ionic contact and thus to a substantial reduction of the effective active surface area, concomitant with an increase in OER overpotential. Nano- and micro-bubbles formed within/near the catalyst layer cannot be removed by rotation, unless they coalesce at the catalyst layer surface from where they can be removed into the bulk of the electrolyte by forced convection. In summary, our data suggest that the increase of the potential in galvanostatic RDE-based stability test is primarily due to a shielding of the majority of the catalyst surface area by evolved O_2 gas rather than due to catalyst degradation/dissolution. Once essentially all of the OER active sites are ionically disconnected by trapped oxygen, the observed potential jump will occur.

A remaining question is why different OER catalysts exhibit different "apparent" stability times in the RDE-based galvanostatic stability test, even in cases where the same catalyst loading and the same geometric current density were used.[13,21,25] While under these nominally identical testing conditions the rate of O_2 evolution is the same, the fraction of the nano- and micro-bubbles accumulating in the porous layer still depends on additional material-specific parameters. These include: i) catalyst layer thickness that depends on the active material (e.g., iridium) packing density; ii) porosity of the catalyst layer (pore size, volume, and connectivity) that depends on catalyst morphology; iii) hydrophobic/hydrophilic properties of the catalyst (i.e., the active material and the support); and, iv) adhesion of the catalyst to the RDE substrate (e.g., gold). Therefore, different catalysts may exhibit different stability times in the RDE-based galvanostatic stability test as long as they are different in at least one of the above listed properties.

Our data undoubtedly explain the inconsistency between stability results from catalysts tested in MEAs (membrane electrode assemblies) in PEM electrolyzers and results from testing the same catalysts in the galvanostatic RDE-based stability test, whereby the apparent catalyst durability in the latter is orders of magnitude shorter than in actual electrolyzers.[26] Furthermore, the results presented in our study also show that the commonly used galvanostatic RDE-based stability test does not provide a measure of catalyst degradation/dissolution, which also puts in question the viability of the reported OER catalyst dissolution rates with respect to electrode potential carried out using half-cells with aqueous electrolytes.[13,21,27–29] Again, this is reflected by the orders of magnitude higher dissolution rates obtained by measurements in liquid electrolyte vs. those in actual PEM electrolyzers.[26]

Conclusions

In this work, we carefully examined the viability of the galvanostatic RDE-based stability test as a tool for benchmarking or even quantifying OER catalyst durability. Although this test has been utilized for several years to compare the stability of various OER catalysts, its results are inconsistent with those obtained from PEM electrolyzers. Our results demonstrate that the galvanostatic RDE-based stability test does not provide a measure of OER catalyst degradation/dissolution. We provide evidence that this is mainly because of the accumulation of oxygen bubbles within the catalyst layer and/or near its interface with the electrolyte, preventing electrolyte contact to the majority of the catalyst surface which reduces the active catalyst surface area and thus gradually increases the OER potential, ultimately leading to a sudden potential jump to very high potentials, which is commonly interpreted as a complete degradation of the catalyst. However, since holding the catalyst for extended time at OCP under argon was shown here to substantially recover catalyst activity and catalyst surface area (measured by cyclic voltammetry), the time until the occurrence of a large potential jump in the galvanostatic RDE-based stability test is not a measure of catalyst degradation, as assumed erroneously in the literature. Therefore, we believe that this test cannot be used to benchmark OER catalyst stability, underlined by the observation that the stability of iridium-based OER catalysts in PEM electrolyzers is tens of thousands of hours in contrast to only hours in the galvanostatic RDE-based stability test.

Acknowledgment

Financial support in the frame of the innoKA project (BMWi, 03ET6096A) is acknowledged. Thanks are extended to Melanie Miller (Department of Chemistry - University of Cambridge, England) for carrying out the very first set of exploratory experiments and for providing the Ir/ATO catalyst for this study. The authors thank Dr. Gregor Harzer, Dr. Armin Siebel, Maximilian Bernt, and Jan Schwämmlein (Chair of Technical Electrochemistry, Technical University of Munich, Germany) for fruitful scientific discussion.

ORCID

Hany A. El-Sayed https://orcid.org/0000-0002-8769-8258

References

1. S. Siracusano, V. Baglio, C. D'Urso, V. Antonucci, and A. S. Aricò, *Electrochimica Acta*, **54**(26), 6292 (2009).
2. V. K. Puthiyapura, S. Pasupathi, S. Basu, X. Wu, H. Su, N. Varagunapandiyan, B. Pollet, and K. Scott, *International Journal of Hydrogen Energy*, **38**(21), 8605 (2013).
3. S. Ferro, D. Rosestolato, C. A. Martínez-Huitle, and A. de Battisti, *Electrochimica Acta*, **146**, 257 (2014).
4. J. Polonský, I. M. Petrushina, E. Christensen, K. Bouzek, C. B. Prag, J. Andersen, and N. J. Bjerrum, *International Journal of Hydrogen Energy*, **37**(3), 2173 (2012).
5. F. Karimi and B. A. Peppley, *Electrochimica Acta*, **246**, 654 (2017).
6. P. Lettenmeier, L. Wang, U. Golla-Schindler, P. Gazdzicki, N. A. Canas, M. Handl, R. Hiesgen, S. S. Hosseiny, A. S. Gago, and K. A. Friedrich, *Angewandte Chemie (International ed. in English)*, **55**(2), 742 (2016).
7. E. Oakton, D. Lebedev, M. Povia, D. F. Abbott, E. Fabbri, A. Fedorov, M. Nachtegaal, C. Copéret, and T. J. Schmidt, *ACS Catal.*, **7**(4), 2346 (2017).
8. H. Ohno, S. Nohara, K. Kakinuma, M. Uchida, A. Miyake, S. Deki, and H. Uchida, *J. Electrochem. Soc.*, **164**(9), F944 (2017).
9. T. Reier, M. Oezaslan, and P. Strasser, *ACS Catal.*, **2**(8), 1765 (2012).
10. S. Zhao, A. Stocks, B. Rasimick, K. More, and H. Xu, *J. Electrochem. Soc.*, **165**(2), F82 (2018).
11. N. H. Kwon, M. Kim, X. Jin, J. Lim, I. Y. Kim, N.-S. Lee, H. Kim, and S.-J. Hwang, *NPG Asia Mater*, **10**(7), 659 (2018).
12. Y.-T. Kim, P. P. Lopes, S.-A. Park, A.-Y. Lee, J. Lim, H. Lee, S. Back, Y. Jung, N. Danilovic, V. Stamenkovic, J. Erlebacher, J. Snyder, and N. M. Markovic, *Nature communications*, **8**(1), 1449 (2017).
13. S. Geiger, O. Kasian, A. M. Mingers, S. S. Nicley, K. Haenen, K. J. J. Mayrhofer, and S. Cherevko, *ChemSusChem*, **41**, 15 (2017).
14. A. S. Aricò, S. Siracusano, N. Briguglio, V. Baglio, A. Di Blasi, and V. Antonucci, *J Appl Electrochem*, **43**(2), 107 (2013).
15. C. Rakousky, U. Reimer, K. Wippermann, M. Carmo, W. Lueke, and D. Stolten, *Journal of Power Sources*, **326**, 120 (2016).
16. K. E. Ayers, E. B. Anderson, K. Dreier, and K. W. Harrison, *ECS Transactions*, **50**(49), 35 (2013).
17. S. M. Alia, B. Rasimick, C. Ngo, K. C. Neyerlin, S. S. Kocha, S. Pylypenko, H. Xu, and B. S. Pivovar, *J. Electrochem. Soc.*, **163**(11), F3105 (2016).
18. H.-S. Oh, H. N. Nong, T. Reier, A. Bergmann, M. Gliech, J. Ferreira de Araújo, E. Willinger, R. Schlögl, D. Teschner, and P. Strasser, *J. Am. Chem. Soc.*, **138**(38), 12552 (2016).
19. S. Geiger, O. Kasian, M. Ledendecker, E. Pizzutilo, A. M. Mingers, W. T. Fu, O. Diaz-Morales, Z. Li, T. Oellers, L. Fruchter, A. Ludwig, K. J. J. Mayrhofer, M. T. M. Koper, and S. Cherevko, *Nat Catal*, **1**(7), 508 (2018).
20. C. C. L. McCrory, S. Jung, J. C. Peters, and T. F. Jaramillo, *Journal of the American Chemical Society*, **135**(45), 16977 (2013).
21. H.-S. Oh, H. N. Nong, T. Reier, M. Gliech, and P. Strasser, *Chem. Sci.*, **6**(6), 3321 (2015).
22. L. Wang, F. Song, G. Ozouf, D. Geiger, T. Morawietz, M. Handl, P. Gazdzicki, C. Beauger, U. Kaiser, R. Hiesgen, A. S. Gago, and K. A. Friedrich, *J. Mater. Chem. A*, **5**(7), 3172 (2017).
23. J. Zhang, G. Wang, Z. Liao, P. Zhang, F. Wang, X. Zhuang, E. Zschech, and X. Feng, *Nano Energy*, **40**, 27 (2017).

24. S. Cherevko, A. A. Topalov, A. R. Zeradjanin, I. Katsounaros, and K. J. J. Mayrhofer, *RSC Adv*, **3**(37), 16516 (2013).
25. H. N. Nong, H.-S. Oh, T. Reier, E. Willinger, M.-G. Willinger, V. Petkov, D. Teschner, and P. Strasser, *Angewandte Chemie (International ed. in English)*, **54**(10), 2975 (2015).
26. S. Cherevko, *Current Opinion in Electrochemistry*, **8**, 118 (2018).
27. S. Cherevko, S. Geiger, O. Kasian, A. Mingers, and K. J. Mayrhofer, *J. Electroanal. Chem.*, **773**, 69 (2016).
28. S. Cherevko, S. Geiger, O. Kasian, A. Mingers, and K. J. Mayrhofer, *J. Electroanal. Chem.*, **774**, 102 (2016).
29. S. Cherevko, T. Reier, A. R. Zeradjanin, Z. Pawolek, P. Strasser, and K. J. Mayrhofer, *Electrochem. Commun.*, **48**, 81 (2014).